ELSEVIER

Chemical Engineering Science 61 (2006) 858–873

Chemical Engineering Science

www.elsevier.com/locate/ces

Lattice Boltzmann simulation of 2D and 3D non-Brownian suspensions in Couette flow

Janneke Kromkamp[a, b, *], Dirk van den Ende[c], Drona Kandhai[d], Ruud van der Sman[a], Remko Boom[a]

[a] *Food and Bioprocess Engineering Group, Wageningen University, Wageningen, The Netherlands*
[b] *Corporate Research, Friesland Foods BV, Deventer, The Netherlands*
[c] *Science and Technology, University of Twente, Enschede, The Netherlands*
[d] *Kramers Laboratorium voor Fysische Technologie, Delft University of Technology, Delft, The Netherlands*

Received 22 March 2005; received in revised form 20 June 2005; accepted 6 August 2005
Available online 23 September 2005

Abstract

In this study, the Lattice Boltzmann (LB) method is applied for computer simulation of suspension flow in Couette systems. Typical aspects of Couette flow such as wall effects and non-zero Reynolds numbers can be studied well with the LB method because of its time-dependent character. Couette flow of single, two and multi-particle systems was studied, where two-dimensional (2D) systems were compared with three-dimensional (3D) systems.

Computations on multi-particle 3D suspensions, for instance to assess the viscosity or shear-induced diffusivity, were found to be very intensive. This was only partly a consequence of the 3D system size. The critical particle grid size, necessary for accurate results, was found to be relatively large, increasing the system to impractical sizes.

It is however demonstrated that it is possible to carry out computer simulations on 2D suspensions and use relatively simple, linear scaling relations to translate these results to 3D suspensions, in this way avoiding intensive computations. By doing so, the LB method is shown to be well-suited for study of suspension flow in Couette systems, particularly for aspects as particle layering near solid walls, hydrodynamic particle interactions and viscous stresses at non-zero Reynolds numbers, which cannot be easily solved with alternative methods. It also opens the way to employ the LB method for other unexplored aspects, such as particle polydispersity and high Reynolds number flow, with large relevance to practical processing of suspensions.

Keywords: Suspension; Lattice Boltzmann method; Computer simulation; Couette flow; Cylinder; Sphere

1. Introduction

Since many manufacturing processes involve the transport of suspensions such as slurries, colloids, polymers and ceramics, knowledge of the flow behaviour of suspensions is of general interest. Not only the behaviour in shear flow but also in the presence of rigid boundaries, such as a pipe wall, is important, because these rigid boundaries can induce effects such as structuring, demixing and wall slip (Komnik and Harting, 2004). In experimental research as well as theoretical research, Couette flow is often used as a means to investigate the suspension flow behaviour in simple shear flow and in the presence of walls.

In the recent years, computer simulation models for colloidal suspension flow have developed into powerful research tools (Ladd and Verberg, 2001). These numerical models take explicit account of the hydrodynamic forces between the suspended particles, although the various models do this in different ways. In Brownian and Stokesian dynamics, the hydrodynamic interactions are assumed to be fully

* Corresponding author. Tel.: +31 570 695917; fax: +31 570 695918.
E-mail address: janneke.kromkamp@frieslandfoods.com (J. Kromkamp).

0009-2509/$ - see front matter © 2005 Elsevier Ltd. All rights reserved.
doi:10.1016/j.ces.2005.08.011

developed. This virtually means that the time scales between the fluid dynamics and the motion of the solid particles are completely separated. These methods are however not suited for suspensions bounded by walls, and are therewith also not suited for Couette flow. Time-dependent models do not assume fully developed hydrodynamic interactions, but take into account the development of hydrodynamic interactions in time and space from purely local stresses generated at the solid-fluid surface. These models, including Lattice Boltzmann (LB) and finite-element methods, as well as particle-based schemes such as dissipative particle dynamics, are suited for describing Couette flow. In comparison to the LB method, finite-element methods require much more computing power, while dissipative particle dynamics is less often used for hydrodynamics. Therefore, the LB method can be considered the best-developed of the time-dependent models for multi-particle suspensions.

In the time-dependent methods, the solid-fluid surface is explicitly present in the system. This mostly means that the solid particles are represented on a numerical grid, which introduces inaccuracy not only in the shape of the particle but also in the fluid flow around the particle. The degree of inaccuracy is dependent on the particle grid size and this brings up limitations in the range of conditions where accurate results can be obtained. One obvious limitation is the volume fraction of particles in the system. Dependent on the particle size, there will be a limiting volume fraction above which the accuracy will be insufficient.

An advantage of computer modelling is that very detailed knowledge on the particle dynamics and structure can be gained, such as the translational and rotational velocities of the individual particles in the suspension. In spite of the large progress in computational power, these computer modelling techniques still require a large computing effort, which limits the system size in the computations. This is particularly the case when the particle grid size needs to be relatively large in order to have sufficient accuracy. One way to reduce the computing power can be to carry out simulations on two-dimensional (2D) instead of three-dimensional (3D) suspensions. Adequate 2D–3D scaling relations are then required to be able to translate the 2D results to predictions for 3D suspensions.

In this paper, we present a study on the use of the LB method for computer simulation of 2D and 3D suspensions in Couette flow, with the aim to investigate whether computer simulations on 2D suspensions can (partly) replace computer simulations on 3D suspensions, especially when the latter are computationally intensive. Hereto, we compare different aspects of the flow behaviour of 2D and 3D suspensions in Couette systems in order to find 2D–3D scaling relations. Furthermore, we investigate the accuracy of the results in relation to the particle size and the volume fraction, as related to the explicit presence of the solid-fluid surface in the system. Therewith, this paper demonstrates the use and the limitations of LB computations on 2D suspensions in Couette flow as compared to 3D real suspensions.

2. Computer simulation method

For general information about the LB method, we refer to literature (see e.g. (Succi, 2001)). In this section, the emphasis is on the suspended particles, their incorporation in the fluid and their interactions.

2.1. Simulation of the fluid

The LB method is based on the well-established connection between the dynamics of a dilute gas and the Navier–Stokes equations (Chapman and Cowling, 1960). In the LB method, the discretised Boltzmann equation is solved for fictitious fluid particles, that are constrained to move on a lattice. The state of the fluid is characterised by the single-particle distribution function $f_i(\mathbf{x}, t)$, describing the average number of particles at a particular node of the lattice $\mathbf{x}$, at a time t, with the discrete velocity $\mathbf{c}_i$, which brings the fluid particles in one time step to an adjacent lattice node. It is known that only a small set of discrete velocities is necessary to simulate the Navier–Stokes equations (Frisch et al., 1986). In the simulations described in this paper, the fluid dynamics were solved with a D2Q9 or a D3Q19 LB scheme, which is, respectively, defined on a 2D square lattice with rest particles and 8 non-zero particle velocities or on a 3D square lattice with rest particles and 18 non-zero particle velocities. The velocity directions link lattice sites to its nearest and next-nearest neighbours. The hydrodynamic field's mass density ρ, momentum density $\mathbf{j}$, and the momentum flux density $\mathbf{\Pi}$ are moments of this velocity distribution:

$$\rho = \sum_i f_i, \quad \mathbf{j} = \sum_i f_i \mathbf{c}_i, \quad \mathbf{\Pi} = \sum_i f_i \mathbf{c}_i \mathbf{c}_i. \tag{1}$$

The fictitious fluid particles and their interactions evolve by collisions and subsequent propagation to neighbouring lattice sites. In a collision step, the distribution function is relaxed towards the local equilibrium distribution according to

$$f_i(\mathbf{x} + \Delta\mathbf{x}_i, t + \Delta t) = f_i(\mathbf{x}, t) - \frac{f_i(\mathbf{x}, t) - f_i^{\mathrm{eq}}(\mathbf{x}, t)}{\tau}. \tag{2}$$

The relaxation time τ controls the relaxation of the viscous stress in the fluid and is linked to the kinematic viscosity ν via:

$$\nu = c_s^2 \left(\tau - \frac{1}{2}\right) \Delta t, \tag{3}$$

where the speed of sound c_s is defined by $c_s^2 = c^2/3$. In our simulations we applied $\tau = 1.0$ (in lattice units), which corresponds to a kinematic viscosity ν of the fluid of $\frac{1}{6}$ (in lattice units). The equilibrium distribution $f_i^{\mathrm{eq}}(\mathbf{x}, t)$ is chosen such that the Navier–Stokes equations for a weakly compressible system are obtained (Qian et al., 1992).

The 2D Couette system consists of a rectangular box with a width X and a height Y (Fig. 1). Periodic boundaries were

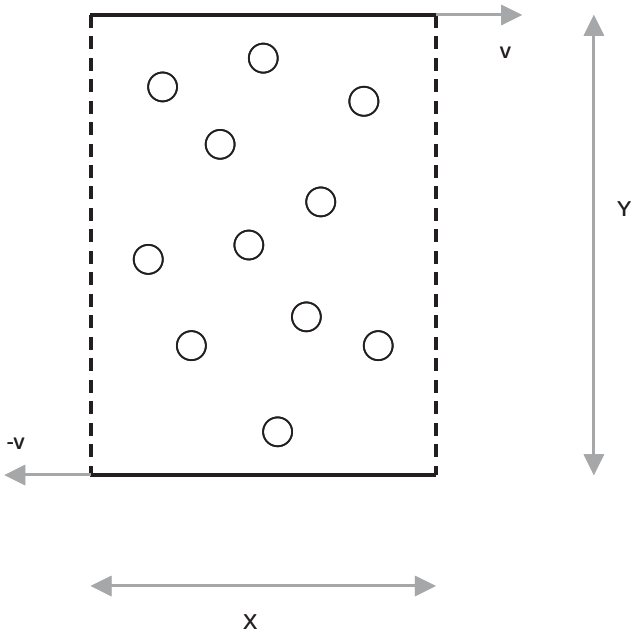

Fig. 1. Schematic representation of the 2D Couette system. The solid box lines represent rigid walls and the dashed lines periodic boundaries. The 3D Couette system is similar, but has an extra dimension *Z*, which is bounded by periodic boundaries.

applied at the left and right side of the box, while the upper and lower boundaries consist of a rigid wall. The rigid walls move with a constant velocity v in a horizontal but opposite direction in order to create a shear flow. The 3D Couette system is similar to the 2D system, but has an extra dimension *Z*, which is bounded by periodic boundaries.

2.2. Fluid–particle interactions

In the LB scheme for particulate suspensions as developed by Ladd (1944a,b), the solid particles are defined by a boundary surface, which can be of any size or shape. The spherical (3D) or circular (2D) particles are projected on the lattice, where the boundary surface cuts off some of the links between lattice nodes. Fluid particles moving along the boundary surface interact with the surface at boundary nodes that are located at the lattice nodes nearest to the boundary surface of the solid particles, following an alternative method to Ladd's, that was developed by Behrend (1995). In this method, called relaxed bounce back conditions at the nodes, the LB collisions are carried out at every node, including the boundary nodes. The method of Behrend avoids some complications of Ladd's method, where additional information is to be passed between lattice nodes because the boundary nodes are placed in between instead of on lattice nodes. The resolution of the particles on the grid is better for Ladd's method. Behrend showed that the translational friction of the particles agreed well with results of Ladd and independent numerical results. The rotational friction however, agreed less well, due to the worse resolution. Comparable results were obtained for the hydrodynamic interactions between pairs of spheres, where the parallel friction coefficients were in excellent agreement with independent numerical solutions, whereas the agreement of the perpendicular friction coefficients was less. Results for three different transport coefficients were all again very accurate.

The collision rules at the boundary surface enforce a stick boundary condition on the fluid, which means that the fluid velocity is matched to the local solid-body velocity $\mathbf{u}_b$. This local solid-body velocity $\mathbf{u}_b$ (at position $\mathbf{x}_b$) is determined by the solid-particle velocity $\mathbf{U}$, its angular velocity $\boldsymbol{\Omega}$ and the position of its center of mass $\mathbf{R}$:

$$\mathbf{u}_b = \mathbf{U} + \boldsymbol{\Omega} \times (\mathbf{x}_b - \mathbf{R}). \tag{4}$$

After the collision phase, the boundary nodes are updated in the following way:

$$f_i(\mathbf{x} + \Delta\mathbf{x}_i, t + \Delta t) = f'_{-i}(\mathbf{x}, t) + \frac{2\rho w_i}{c_s^2}\,\mathbf{u}_b \cdot c_i, \tag{5}$$

$$f_i(\mathbf{x} - \Delta\mathbf{x}_i, t + \Delta t) = f'_i(\mathbf{x}, t) - \frac{2\rho w_i}{c_s^2}\,\mathbf{u}_b \cdot c_i. \tag{6}$$

For moving suspension particles, in this update, momentum is exchanged between the incoming particles from the fluid and the solid side (the combined momentum of the fluid and the solid phase is however conserved). From this momentum exchange the force and torque exerted on a suspension particle is calculated. Hereafter the kinematic properties of the suspension particles themselves are updated with a simple Euler forward integration of Newton's second law.

The calculations on spherical (3D) and circular (2D) particles follow essentially the same method. Only the mass M and the moment of inertia I in Newton's second law differ. For 3D particles, they are given by

$$M = \rho_s \tfrac{4}{3}\pi a^3, \tag{7}$$

$$I = 0.4Ma^2, \tag{8}$$

where ρ and ρ_s are the density of the fluid and the solid particle, respectively, and a is the particle radius. For 2D particles, M and I are given by

$$M = \rho_s \pi a^2, \tag{9}$$

$$I = 0.5Ma^2. \tag{10}$$

Since a suspended particle is essentially simulated by the introduction of a boundary surface, separating the interior of the particle from the exterior, the interior of the particle also consists of fluid. The particles thus comprise a solid shell of given mass and inertia, filled with fluid of the same mass density as the bulk fluid. Ladd (1994b) examined the effects of the interior fluid on the behaviour of the particle. Dynamically, the particle behaves as if its mass is the sum of the shell mass and the mass of the interior fluid. With a sufficiently high effective mass of the shell, the contribution of the interior fluid to the inertial force is negligibly small.

Our computations were carried out in this regime, with an effective mass ρ_s/ρ of 10. Since our computations are carried out in the Stokes flow regime, inertial effects do not play a role (see also Kromkamp et al. (2005)).

2.3. Accuracy of particle representation and particle–particle interactions

By the projection of the suspended particles on the lattice, a discrete representation of the surface is obtained, which becomes more and more precise as the surface curvature gets smaller and which is exact for surfaces parallel to lattice planes. Together with the choice of the location of the boundary nodes and the boundary update rules, the discretisation of the particle surface onto the lattice induces a hydrodynamic particle diameter that is slightly larger than the diameter based on the number of occupied lattice nodes (Ladd, 1994b). It is therefore often proposed that the particle diameter should be corrected for this hydrodynamic effect. The magnitude of the correction is mostly based on the particle behaviour in the Stokes flow regime and at low particle concentrations. As also presented in an earlier paper (Kromkamp et al., 2005), we have seen that in suspensions in shear flow, particles can approach each other very close, such that particles would largely overlap when the hydrodynamic particle size would be taken into account. The closest approach distance is moreover found to be dependent on conditions such as the particle concentration and the shear rate. Since assessment of the hydrodynamic particle diameter in these systems is virtually impossible, while the corrections would probably be very small, we did not apply this correction but used the input particle diameter in our calculations.

Since the suspension flow behaviour in Couette systems is mainly governed by hydrodynamic particle–particle or particle–wall interactions, these interactions need to be accurately resolved in the computations. When two suspension particles come into close contact with each other, the lubrication force becomes important. This force is caused by the attenuation of the fluid film in the gap between the two particles and is repulsive upon approach and attractive upon separation of the particles. When the gap width between two particles is in the order of one lattice spacing, the lubrication force is however not exactly resolved with the LB method. This is due to the discretisation of the particles and fluid on a grid and is a problem that is encountered by all numerical methods. This lubrication breakdown leads to a so-called "depletion force" that pushes particles into each other. To overcome this problem we applied a lubrication correction method based on an explicit calculation of the lubrication force F (Nguyen and Ladd, 2002). For a 3D system F is given by (Nguyen and Ladd, 2002):

$$F = -6\pi\eta \mathbf{U}_{12}.\hat{\mathbf{R}}_{12}\frac{a_1 a_2}{(a_1+a_2)^2}\left(\frac{1}{h}-\frac{1}{h_c}\right), \quad h<h_c,$$

$$F = 0, \quad h>h_c, \tag{11}$$

where η is the viscosity, $\mathbf{U}_{12}=\mathbf{U}_1-\mathbf{U}_2$, $h=|\mathbf{R}_{12}|-(a_1+a_2)$ is the gap (distance between the particle surfaces) and h_c represents the cut-off distance between the particle surfaces for the added lubrication force. The unit vector $\hat{\mathbf{R}}_{12}=\mathbf{R}_{12}/|\mathbf{R}_{12}|$. For a 2D system the lubrication force per unit cylinder length F is given by (see Appendix A):

$$F = -\frac{1}{2}\eta \mathbf{U}_{12}.\hat{\mathbf{R}}_{12}\left(\left(\frac{a_1+a_2}{h}\right)^{3/2}\left(F_0+\frac{h}{a_1+a_2}F_1\right)-\left(\frac{a_1+a_2}{h_c}\right)^{3/2}\left(F_0+\frac{h_c}{a_1+a_2}F_1\right)\right),$$

$$h<h_c,$$

$$F = 0, \quad h>h_c, \tag{12}$$

where F_0 is the numerical constant $\frac{3}{4}\pi\sqrt{2}=3.3322$ and F_1 is the first order correction for the lubrication limit $h/2a \ll 1$ with a value of $\frac{231}{80}\cdot\pi\cdot\sqrt{2}=12.829$. In accordance with Ladd and Verberg (2001), we applied a correction on the lubrication force to account for the lubrication force that is already resolved in the computations of the fluid dynamics. This was done by subtracting the lubrication force at a cut-off distance h_c from the total lubrication force, as indicated in Eqs. (11) and (12). For the added lubrication force, the cut-off distance h_c between the particle surfaces was chosen equal to 1.1 lattice units for a 3D system and to 2.0 lattice units for a 2D system (as was found optimal in our simulations). For 3D systems, Nguyen and Ladd (2002) showed that this correction leads to more accurate results for particle interactions at short interparticle distances, even with neutrally buoyant particles very near to contact and without causing instabilities in the particle dynamics.

In a similar way, the tangential lubrication can also be corrected. Since it has a weaker logarithmic divergence and its breakdown does not lead to serious problems, we have not included this correction in our simulations.

We have noticed before, that in suspensions with relatively high particle fractions or at high particle Reynolds number, particle clustering and overlap can occur, which greatly affects the diffusive behaviour of the particles (Kromkamp et al., 2005). This behaviour seems to be correlated with the lubrication breakdown of concentrated colloids, that was reported by Ball and Melrose (1995). As suggested by these authors, we applied a Hookean spring force between the particles to avoid this clustering and overlap. This Hookean spring force was applied for gaps h smaller than a thickness δ and was applied in the direction of the line of particle centres, according to

$$F_h = F_0 - \left(\frac{F_0}{\delta}\right)h \tag{13}$$

with a maximal Hookean spring force F_0 of 2.5×10^{-6} (in lattice units) for a 3D system and 10.0 (in lattice units) for

a 2D system. The Hookean spring force is active in a layer around the particle with a thickness $\delta/2$ of 0.025 lattice units for a 3D system and 0.05 lattice units for a 2D system.

3. Single and pair particles in Couette flow

3.1. Wall effects on a single particle

In order to compare wall effects between a single suspended 2D particle and a 3D particle in shear flow, the rotation was studied in Couette systems with varying ratio of channel height to particle radius Y/a. For 3D particles, we take the data from Nirschl et al. (1995), who used a finite volume numerical scheme. We studied the rotation of 2D particles with our LB model.

The LB calculations were carried out for a 2D particle with a radius a of 8 lattice units. The distance X/a between the periodic boundaries was 80, which was verified to give results corresponding to a system with an infinitely large distance X/a. The channel height Y/a varied between 2.5 and 40. The shear rate $\dot{\gamma}$ was 3.75×10^{-5} per time step, which was verified to give results corresponding to Stokes flow. The shear-based particle Reynolds number $Re_{\text{shear},p} = 4\dot{\gamma}a^2/v$, where v is the kinematic viscosity, was equal to 0.058. The 2D particle was placed at the horizontal centerline of the Couette system. We assessed the equilibrium angular velocity ω of the 2D particle, which is normalised for the shear rate.

For a channel height Y/a larger than 10, the angular velocity ω was close to the analytical solution of Taylor (1932) for a rotating particle in simple shear (Fig. 2). For smaller channel heights, the angular velocity ω starts to decrease due to interaction with the walls. The decrease starts earlier and is most pronounced for the 2D particle, where the angular velocity ω decreased from the maximum value of 0.50 to a value of 0.33 at a channel height Y/a of 2.5. This effect can be understood because the intensity of the flow field around a 2D particle is larger than around a 3D particle. As a result, for 2D particles, wall effects start at a channel height Y/a, which is about 3 units higher than for 3D particles, while the wall effects for 2D particles are more intense as well. The results suggest that a scaling can be obtained between 2D and 3D results by normalisation of the channel height. For the 2D results, the channel height should be multiplied with a factor of about 0.33.

3.2. Two colliding particles in shear flow

The hydrodynamic interactions between particles in a 2D and a 3D system can be compared from the flow trajectory of two interacting particles. Batchelor and Green (1972) have derived an analytical solution for 3D particles, but a solution for 2D particles is not yet available. Therefore, we calculated the flow trajectories with the LB model for 2D as well as 3D particles, at equivalent conditions.

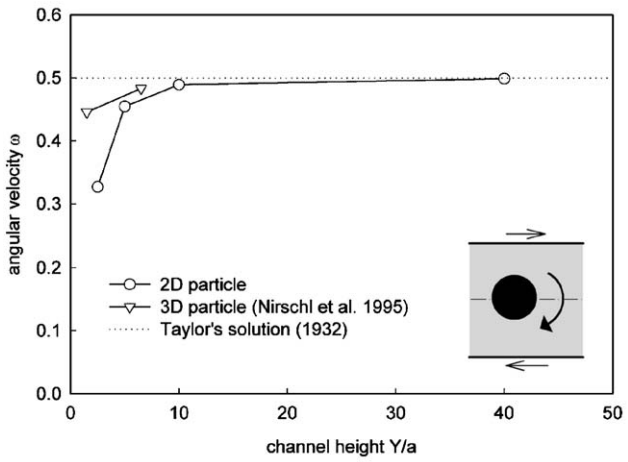

Fig. 2. The angular velocity ω as a function of the relative channel height Y/a for a single cylinder with radius a in shear flow ($Re_{\text{shear},p} = 0.058$, $a = 8$ lattice units). The distance between the solid walls of the Couette system was varied between $2.5a$ and $40a$. The results are compared to results of Nirschl et al. (1995) for a 3D system. The inset shows a scheme of the simulated situation.

For 2D particles, two equal-sized particles ($a = 8$ lattice units) were placed at equidistant heights above and under the horizontal centerline. The initial horizontal distance $(x - x_{\text{midpoint}})/a$ from the midpoint between the particles was 5, while the initial vertical distance was varied. Both the channel height ($Y/a = 40$) and the distance between the periodic boundaries ($X/a = 80$) were chosen such that they did not affect the particle trajectories. $Re_{\text{shear},p}$ was equal to 0.058, which was verified to give results in accordance with Stokes flow. For 3D particles, virtually the same conditions are applied, except for the particle radius, which was chosen as 11 lattice units.

The resulting flow trajectories are presented in Fig. 3. When the two particles pass each other, they move away from the horizontal centerline upon approach and move back to their original height upon separation, as is described by Batchelor and Green (1972). When comparing 2D and 3D particles, it is clear that the 3D particles move closer around each other: the minimal gap between the 2D particles is equal to $0.27a$ and $0.11a$ for initial vertical distances from the midpoint of, respectively, $0.44a$ and $0.25a$, while the minimal gap between 3D particles is, respectively, $0.01a$ and $0.00a$.

These differences between the inter-particle distances are caused by differences between the ratio of drag to lubrication force for 2D and 3D particles, which causes the fluid to move less easily out of or into the gap for 2D particles. A consequence of the observed behaviour is that the range of hydrodynamic interactions is longer for 2D particles. In 2D multi-particle systems, this may lead to more intense hydrodynamic interactions at a similar particle fraction.

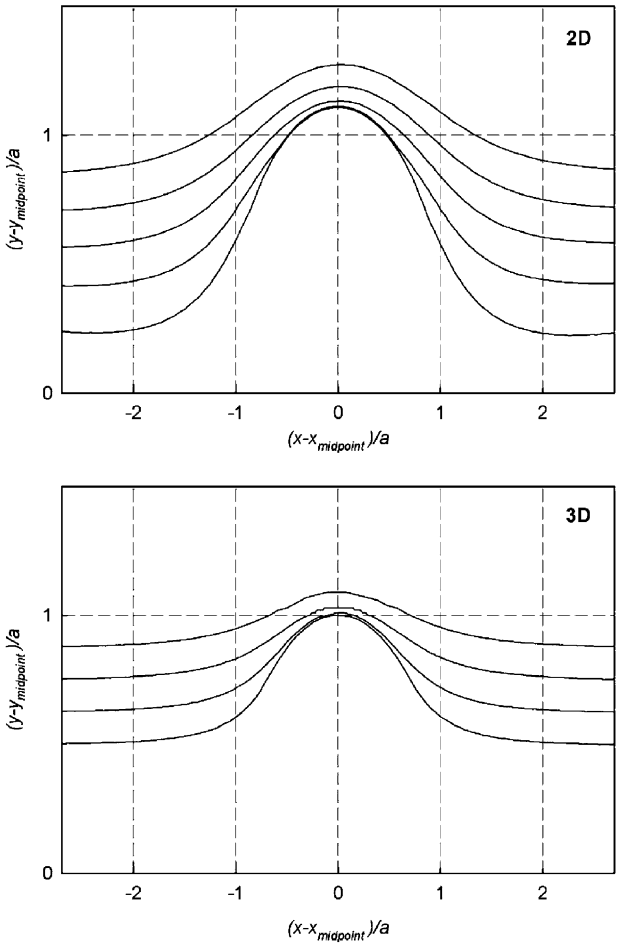

Fig. 3. Cylinder or sphere trajectory during interaction of two cylinders ($a = 8.0$ lattice units (2D)) or two spheres ($a = 11.0$ lattice units (3D)) in a linear shear field ($Re_{\text{shear},p} = 0.058$) between two walls, for varying initial positions of the cylinders and spheres.

A full scaling of the particle trajectories would at least require a numerical solution of the lubrication force, but here we apply an analytical scaling by simply rescaling of the X-axis and Y-axis in Fig. 3. The X-axis is rescaled by normalising X for X_*, the X-value where the particle has reached a distance $Y_* = 0.5(Y_{\max} - Y_{\text{initial}})$. The Y-axis is rescaled by normalising Y for the factor $Y_{\max}(Y - Y_{\text{initial}})/(Y_{\max} - Y_{\text{initial}}) + 1.0(Y_{\max} - Y)/(Y_{\max} - Y_{\text{initial}})$. Obviously, this rescaling can only be applied when X_* and $Y_{\max}$ are already known. The result is presented in Fig. 4.

The rescaling lead to 2D and 3D trajectories with a good resemblance, except when the particles are relatively far apart. These long-range effects are often less relevant in concentrated suspensions. This indicates that the trajectories of 2D and 3D systems can be scaled with the parameters X_* and $Y_{\max}$, which can thus be considered characteristic for this system.

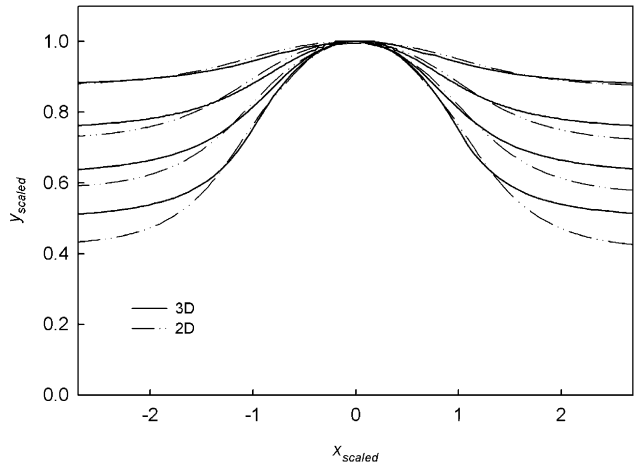

Fig. 4. Cylinder or sphere trajectory during interaction of two cylinders ($a = 8.0$ lattice units (2D)) or two spheres ($a = 11.0$ lattice units (3D)) in a linear shear field ($Re_{\text{shear},p} = 0.058$) between two walls, for varying initial positions of the cylinders and spheres. The values for X and Y are scaled as explained in the text (Section 3.2).

4. 2D and 3D multiparticle suspensions in Couette flow

4.1. Wall effects

The 2D multiparticle system consists of a rectangular box with $X : Y = 1 : 2$. The total number of particles (particle radius 8 lattice units) was equal to 200. $Re_{\text{shear},p}$ was equal to 0.023. In the 3D multiparticle system, the particle radius and $Re_{\text{shear},p}$ were similar to the 2D system. The box size was $X : Y : Z = 1 : 1.5 : 1$ and the total number of particles 400.

Walls can induce effects as particle structuring, demixing and wall slip. In order to analyse these effects, we compare the time-averaged concentration distribution and the particle velocity profile as a function of the distance to the wall for 2D and 3D systems (Fig. 5). In the 2D system, a layer near the walls with a height close to a was depleted of particles, as can be expected based on the particle size. No additional wall depletion was however found. For $\phi > 0.10$, strong structuring effects are found near the walls, which is clear from the concentration fluctuations at these places. The first concentration peak appears for a distance from the wall between 0 and $1.3a$ for $\phi = 0.3$ and between $1.1a$ and $2.1a$ for $\phi = 0.45$. For $\phi = 0.45$ at least two distinct particle layers are visible, at a distance between $1.1a$ and $2.1a$ and between $3.2a$ and $4.2a$ from the wall, respectively. From the particle velocity profile in the 2D system, it is clear that the shear profile deviates slightly from perfectly linear, but that, even for $\phi = 0.45$ where the particle velocity near the walls was up to 5% smaller than expected, this effect of wall slip is of minor importance.

In a 3D system, the situation was slightly different (Fig. 5). The height of the layer near the walls that was depleted of particles, was again close to a. Structuring effects

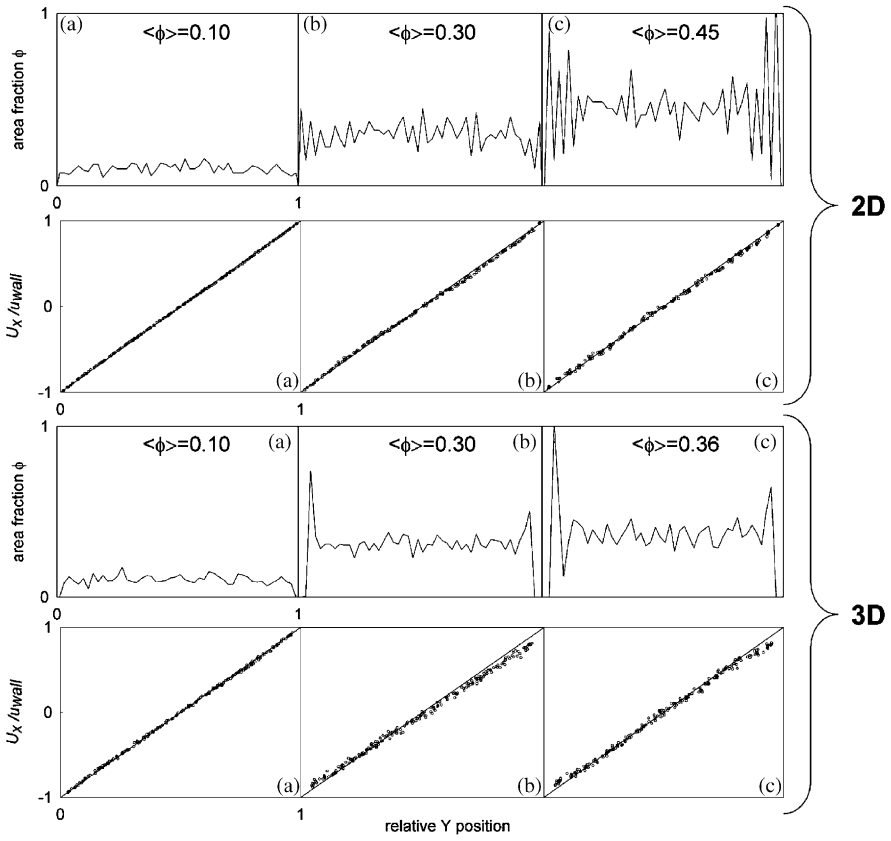

Fig. 5. The time-averaged area (2D, cylinders) or volume (3D, spheres) fraction ϕ across the channel width Y for a 2D suspension (top) with mean area fractions $\langle\phi\rangle$ of 0.10 (a), 0.30 (b) and 0.45 (c) and a 3D suspension (bottom) with mean volume fractions $\langle\phi\rangle$ of 0.10 (a), 0.30 (b) and 0.36 (c).

were found to differ from 2D systems. In 3D systems, for volume fractions higher than 0.10, only one concentration peak was visible, which was more pronounced than in 2D systems. For $\phi = 0.3$, and 0.36 this concentration peak appears at a distance from the wall between $0.93a$ and $1.40a$ and between $0.88a$ and $1.09a$, respectively. As in accordance with wall effects in a single particle system, where wall effects on 3D spheres were only evident at small channel heights when compared to 2D cylinders, the concentration peak was closer to the wall in a 3D system (at the highest concentration). As a consequence of this more pronounced structuring in 3D systems, the particle velocity profile was also found to deviate more from perfectly linear. The profile exhibited a tendency towards a sigmoid shape. The velocity of particles near the walls deviated around 10% from the velocity expected for a linear velocity profile.

4.2. Viscosity

The viscosity of a concentrated suspension is a characteristic that strongly depends on hydrodynamic interactions. By calculation of the squeezing flow contribution, the viscosity can be calculated as a function of the particle fraction, as is done for 3D particles by Frankel and Acrivos (1967). The result is practically identical to the semi-empirical model of (Krieger, 1972; Krieger and Dougherty, 1959), which is valid for both 2D and 3D suspensions:

$$\eta_r = \left(1 - \frac{\langle\phi_s\rangle}{\phi_{\max}}\right)^{-[\eta]\phi_{\max}}, \tag{14}$$

where η_r is the relative viscosity, $\langle\phi_s\rangle$ is the averaged particle fraction and $\phi_{\max}$, the maximum packing fraction. The dimensionless factor $[\eta]$ is the intrinsic relative viscosity of the suspension. It is often suggested that the factor $[\eta]\phi_{\max}$ is similar for 2D and 3D suspensions (Shakib-Manesh et al., 2002). Here we will use $[\eta]\phi_{\max} = 1.82$, as follows from the values for $\phi_{\max}$ and $[\eta]$ of 2.68 and 0.68, respectively, that are reported by Phillips et al. (1992) for 3D suspensions. The value for $\phi_{\max}$ followed from a fit of the simulation results.

Because the viscosity simply evolves from the lubrication force as a function of the mean distance between the particles, the scaling relation between 2D and 3D systems directly follows from this derivation. Therefore, we only determined the viscosity as a function of the particle fraction to compare the accuracy between 2D and 3D systems. In our simulations, the viscosity is determined from the stress at the walls in a multiparticle Couette system. For a 2D system, the height Y/a and width X/a of the Couette system are equal

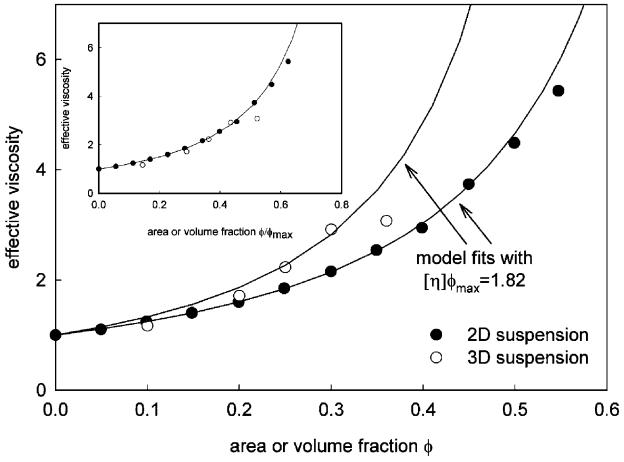

Fig. 6. Effective viscosity of a 2D and a 3D suspension as a function of the area (cylinders) or volume (spheres) fraction. The lines represent fits of the results to the Krieger–Dougherty model with a value of 1.82 for $[\eta]\phi_{\max}$, both for 2D and for 3D suspensions (the fit result for $\phi_{\max}$ was 0.88 for 2D and 0.69 for 3D). The inset shows the viscosity as a function of $\phi/\phi_{\max}$.

to, respectively, 64.75 and 32.38. The particle fraction was varied by varying the amount of particles up to a maximum of 365. $Re_{\text{shear},p}$ was equal to 0.012, which was verified to give results in accordance with Stokes flow. For a 3D system, the system properties were as described in Section 4.1.

Fig. 6 presents the results. There is a good agreement between the 2D computer simulation results and the Krieger–Dougherty model for $\phi_{\max} = 0.88$. At a particle fraction ϕ exceeding 0.49 however, the viscosity is slightly lower than according to the Krieger–Dougherty model. Also the 3D computer simulation results show a good agreement with the Krieger–Dougherty model ($\phi_{\max} = 0.69$). Similar to the 2D system, at higher concentrations, the viscosity starts to get lower than the Krieger–Dougherty model. This occurs however at a particle fraction ϕ exceeding 0.3 instead of 0.49 for a 2D system. From comparison of our 2D viscosity data with LB results from literature (see e.g. Shakib-Manesh et al., 2002 for an overview), it is clear that our data do not significantly differ from these data. 3D viscosity data are amongst others given by Heemels et al. (2000). These authors could accurately describe the viscosity up to a volume fraction of at least 0.45, making use of the similar LB method as Ladd, but adapted in order to simulate truly solid particles. They also showed that when the original LB method of Ladd is used Ladd (1994a,b), the internal fluid in the particles contributes to the effective density, which leads to an underestimation of the viscosity over the total volume fraction regime. A leveling off at higher volume fractions, as occurs in our simulations, is however not observed. Because this behaviour is found at lower volume fractions in 3D suspensions, where the particles come into closer contact, we hypothesize that the inaccuracy in the viscosity has to do with this close contact. It may therefore be that the less accurate particle representation, that is associated with Behrend's boundary rules as used in this study, is the main reason for the inaccuracy at higher particle fractions. The viscosity results indicate that particle radii in concentrated 3D suspensions should be relatively large in order to obtain sufficient accuracy. Since 3D suspensions require much computing power, this is a clear disadvantage of the method followed. From Fig. 6, it is however clear that an appropriate scaling is obtained when the particle fractions of both 2D and 3D suspensions are related to $\phi_{\max}$.

4.3. Shear-induced diffusion

4.3.1. Computer simulation

Another interesting phenomenon in multiparticle suspensions in shear flow is shear-induced diffusion, a phenomenon that arises from the hydrodynamic interactions between the particles. As can be seen in Fig. 3, apart from the displacement caused by the affine flow, two-particle interactions do not lead to permanent displacements of these particles. In a concentrated multi-particle suspension however, simultaneous interactions between more than two particles can lead to permanent displacements, which can have a diffusive character on a sufficiently large timescale. The shear-induced self-diffusivity is thus defined as the time rate of change of one half times the mean-square displacement:

$$D_{xx} \equiv \lim_{t\to\infty} \frac{1}{2}\frac{\mathrm{d}}{\mathrm{d}t}\langle x(t)x(t)\rangle. \tag{15}$$

Sierou and Brady (2004) have done extensive computer simulation work on shear-induced self-diffusion, using the Stokesian dynamics technique. Although in the past, the system size was severely limited because of limits in the computing capacity, as far as we know, they have not published any results from 2D simulations. In contrast to Stokesian dynamics, our LB method enables research on shear-induced diffusion at non-Stokesian conditions, such as in the presence of walls and at non-zero Reynolds number. Here, we investigate 2D–3D scaling relations for shear-induced diffusion because this knowledge may enable the use of computationally less intensive 2D simulations.

The 2D and 3D systems were as described in Section 4.1. For a 2D system, the shear-induced diffusivity is determined over a strain range between 18 and 60. In order to evaluate the effect of the initial particle configuration on the diffusion coefficient, we splitted the displacement curve of one simulation run into several curves which start at different times of the simulation run (and consequently at different particle configurations). In each separate curve, the mean square displacement was monitored over a strain of 30. The final diffusion coefficient is the mean value of the diffusion coefficients that were determined from the individual mean square displacement curves. Dependent on the particle volume fraction, the 2D calculations required between 70 and 650 h CPU time. With a similar particle radius, the 3D system requires much more computational power per

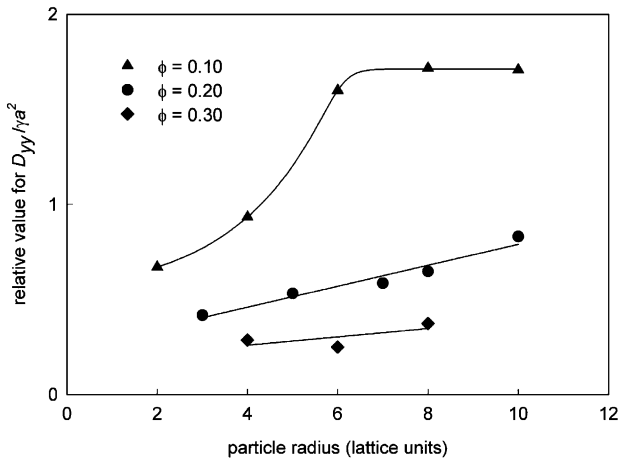

Fig. 7. Component D_{yy} of the shear-induced self-diffusion coefficient, as related to the values found with Stokesian dynamics (Sierou and Brady, 2004), in a 3D suspension as a function of the particle radius for ϕ=0.10, 0.20 and 0.30 ($N = 400$, $Re_{\text{shear},p} = 0.023$). The lines are drawn as a guide to the eye.

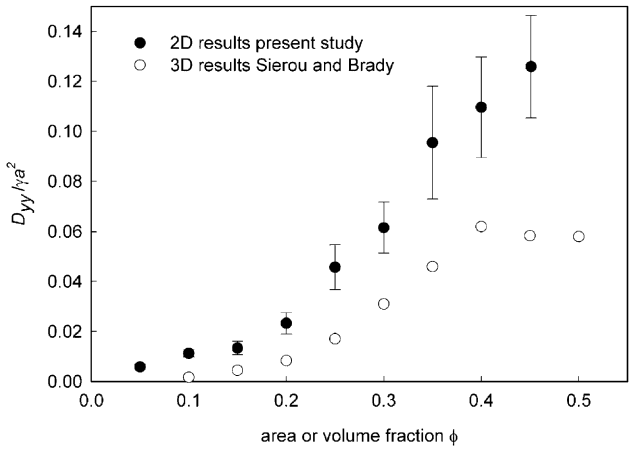

Fig. 8. Component D_{yy} of the shear-induced self-diffusion coefficient as a function of the cylinder area fraction for a 2D suspension ($N = 200$) in shear flow at $Re_{\text{shear},p} = 0.023$. The open symbols represent the relation found by Sierou and Brady (2004) for a 3D system with spheres instead of cylinders.

simulated particle than a 2D system. For 3D systems, a particle number of 400 is found to be sufficiently high to obtain results that are representative for an infinitely large system. This particle number was twice as high as in a 2D system, which results in an improved statistical reliability of the 3D simulations. In order to limit the computational effort, the shear-induced diffusivity is determined over a strain range between 4.5 and 15, which was verified to give results representative for the long-range diffusive regime. In this way, the 3D simulations required about 40 times more CPU time than the 2D simulations (with equal particle radius).

For a 3D system and $\phi \geqslant 0.20$, our simulations generated shear-induced diffusivities that are smaller than the results found by Sierou and Brady (2004). In order to try to elucidate these differences, we assessed the influence of the particle radius on the shear-induced diffusivity at $\phi = 0.10$, 0.20 and 0.30 (Fig. 7).

The shear-induced diffusivity increased with the particle radius, but seems to have reached a plateau value for ϕ=0.10 at a particle radius of 8 lattice units. For ϕ=0.20 and 0.30, even at a particle radius of 10 lattice units, a plateau value was not reached. The values for $\phi = 0.30$ were furthermost away from the values presented by Sierou and Brady.

One hypothesis for the cause of the differences could be that a jammed state of hydrodynamic clusters is formed, as for instance put forward by Farr et al. (1997). Because the particles have more or less fixed positions in such system-spanning clusters, the particle displacements may be smaller than in an unjammed state. It can be expected that system size will be of large influence on the jamming transition. We did however not find these effects when varying the distance between the two moving walls. Therewith, this hypothesis is less likely to be the cause for the differences in shear-induced diffusivity.

Another reason might be in the occurrence of short-range multi-particle interactions. In our code, multi-particle interactions are solved by pair-wise calculation of the interaction effects, which are successively calculated for all particle pairs. The problem does not seem to be in the pair-wise calculation itself, because this would not lead to an effect of the particle radius as shown in Fig. 7. It may however be that the solution of the short-range multi-particle interactions in our code is too inaccurate because of the ragged particle surface. This explanation is in line with the observed effect of the particle radius and our hypothesis based on the viscosity results. Because of the relative close approach of particles in 3D systems, this problem might be more pronounced in 3D than in 2D systems.

Since the inaccuracy is found to increase with ϕ, it can be expected that for volume fractions higher than 0.20, even larger particles are required. However, a particle radius of 14 would already require about 2000 times more CPU time than 2D simulations, while the CPU time would increase with a factor of about 25,000 for a particle radius of 20. Even on advanced supercomputers, one would run into problems with these requirements.

The 2D results on shear-induced diffusivity are presented in Fig. 8. These results were not found to be dependent on the particle size within a range of ±25%. We can thus conclude that, similar to the viscosity results, the 2D results for shear-induced diffusion are less sensitive to inaccuracy in the particle representation on the grid. At area fractions higher than 0.45 however, very large standard deviations were found, which may be caused by comparable reasons as mentioned above for 3D systems, namely formation of a jammed state or inaccuracies in the calculation of the short-range multi-particle interactions. Therefore, we limited the results up to an area fraction of 0.45.

The relation between shear-induced diffusivity and ϕ is clearly different from the 3D relation. For volume fractions lower than 0.25, the 2D shear-induced diffusivity was around three times higher, and at higher fractions around two times. In order to better understand these differences and to be able to translate 2D results into 3D results, we have developed an analytical model for shear-induced diffusivity. This model is discussed in the next section.

4.3.2. Analytical model for 2D–3D scaling

We used an analytical model for shear-induced diffusion (an adapted version of the model that was originally published by Breedveld (2000)), which is based on a simple collision mechanism. Just as most other analytical models, our analytical model does not give an accurate quantitative prediction of shear-induced self-diffusion, but because it captures the volume fraction dependence rather well, we found it relevant to apply it for a comparison between 2D and 3D systems.

Our simple collision model, described in Appendix B, approaches self-diffusion in a similar way as Leighton and Acrivos (1987) did. It describes the movement of individual particles in a homogeneous suspension and shear field under the action of excluded volume effects that are caused by interactions with neighbouring particles on different streamlines in the shear flow. The particle motion during each encounter is described as a deterministic process, but it is assumed that this can lead to diffusive behaviour in systems with many particles and random initial positions. An encounter of particles is modelled as an effective two-particle collision process, which proceeds unhindered until it is terminated by the presence of a third neighbouring particle. Without the presence of a third neighbouring particle, the collision is ended when the angle $\theta = \pi$ is reached (see figure in Appendix), which does not result in a net displacement of the colliding particle. This is consistent with the shear flow trajectories that are obtained in the symmetric problem of two colliding ideal hard spheres (Da Cunha and Hinch, 1996). When particle concentrations are high, the average time between subsequent collisions is shorter than the time needed to complete the interaction and then the collisions end when interaction with a third incoming particle occurs. Under these model assumptions, in a following step, particle trajectories are calculated as a function of initial particle positions and finally, averaging the displacements over all configurations provides a measure for shear-induced self-diffusion. It is clear that the model will be valid for a restricted range of particle fractions. This range is determined by factors such as the presence of two-particle interactions and the homogeneity of the suspension. In previous work (Kromkamp et al., 2005), we have seen that particles in an inhomogeneous suspension can have an increased shear-induced diffusivity. But, although the model is simplistic in that it does not at all consider complex hydrodynamics, it provides interesting insights into the nature of the microscopic processes that could be responsible for shear-induced self-diffusion, even more because the model does not contain adjustable parameters.

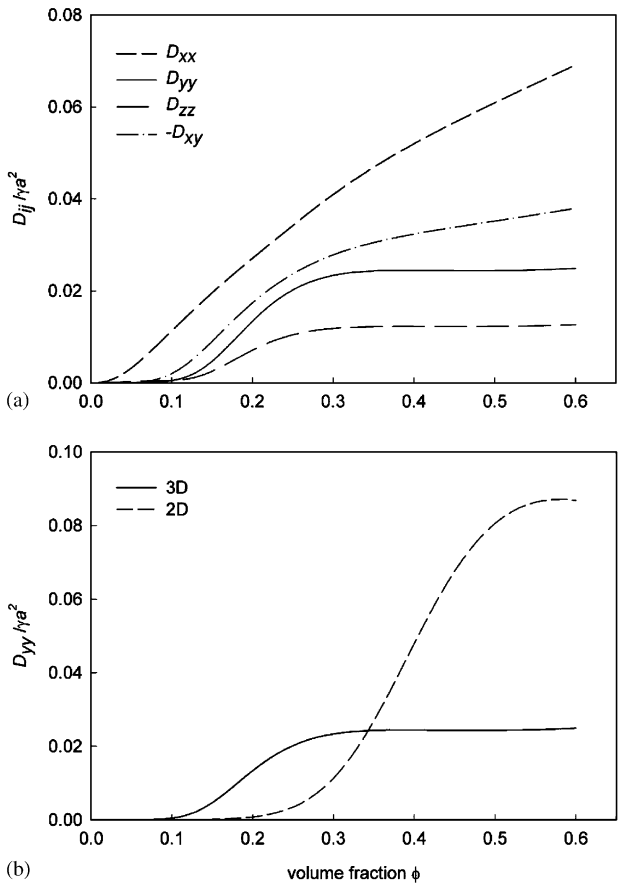

Fig. 9. The components D_{xx}, D_{yy}, D_{zz} and D_{xy} of the diffusion tensor for a 3D system, as calculated from the collision model (part a) and D_{yy} for a 2D system as compared to a 3D system (part b).

With our collision model, the components D_{xx}, D_{yy}, D_{zz} and D_{xy} of the diffusion tensor have been calculated for a 3D system (Fig. 9). The calculated values for the components D_{yy} and D_{zz} are almost a factor 4 lower than most experimental data (see e.g. (Breedveld et al., 1998, 2001)). The latest numerical results, calculated with ASD, are however also a factor 2 lower than experimental data; it was postulated by the authors that discrepancies are due to analysing over too short strains in the experiments (Sierou and Brady, 2004). The difference between the collision model and the numerical values for D_{yy} was around a factor 2.

A feature that seems to be captured well by the collision model is the volume fraction dependence. D_{yy} and D_{zz} level off for volume fractions above 25%. In the model, this is due to the fact that above this critical concentration, the average duration of an interaction is shorter than needed for the completion of the trajectory to $\theta = \pi$. The diffusion components D_{yy} and D_{zz} reach a plateau value at this volume fraction

of 25%. This is due to the fact that the decrease in displacement with higher volume fraction is exactly balanced by the increase in collision frequency, resulting in constant diffusion coefficients. Such a plateau value for D_{yy} and D_{zz} is also found in experiments, although at a somewhat higher volume fraction of around $\phi = 0.35$. Most model predictions however do not show a plateau value at all. Only Sierou and Brady (2004) found a plateau value for D_{yy} as well as D_{zz} in their latest model calculations with the ASD technique. Therefore, it is remarkable that our simple collision model does show this plateau value.

The anisotropy D_{yy}/D_{zz} between the velocity gradient and vorticity direction is equal to 2 in our model. The value of 2 agrees well with experimentally observed values for the anisotropy D_{yy}/D_{zz}. Although only a limited number of results on D_{xx} and D_{xy} is available in literature, it seems clear that the results of our collision model exhibit large differences with these results. Particularly the volume fraction dependence is different in our model results. The negative sign of D_{xy} is however correctly predicted. Since considerable debate still exists on the magnitudes of D_{xx} and D_{xy}, it is hard to assess the accuracy of the model predictions. With respect to D_{xx} and D_{xy}, the subject clearly needs more elucidation.

For a 2D system, the collision model predicts a different volume fraction dependence of D_{yy} than for a 3D system (Fig. 9). At first, D_{yy} only starts to increase at an area fraction between 0.2 and 0.3. After it has started increasing however, the diffusion component D_{yy} not only increases faster with the area/volume fraction, but it also reaches its plateau value at a critical value, which is two times higher than for a 3D system. Moreover, at area fractions above the critical value, the diffusion component exhibits a decrease instead of staying at a constant level. A relevant factor for these differences is the collision rate per particle. In a 2D system, the collision rate per particle at a certain fraction is two times smaller than in a 3D system. On the other hand, the average displacement during a collision is larger because the angle φ is equal to 0 in 2D systems, resulting in the maximal value of 1 for $\cos(\varphi)$. The combination of these two effects leads to a somewhat steeper increase of D_{yy} with the area/volume fraction than in 3D systems, although the difference is not large. The smaller collision rate per particle in 2D systems is also relevant for the onset concentration of D_{yy} and the critical concentration where levelling off occurs. The onset concentration is directly related to the collision rate, because it is determined by the point where a two particle collision starts to be disturbed by a third particle. For the critical concentration, the average collision time is also important. Since the average time needed for a collision does not differ much between 2D and 3D systems, the smaller collision rate causes a shift of the critical concentration from 0.25 to about 0.50 in 2D systems. At higher concentrations in 2D systems, the effect of decreasing displacement is larger than the effect of increasing collision rate, leading to a net decrease of D_{yy}.

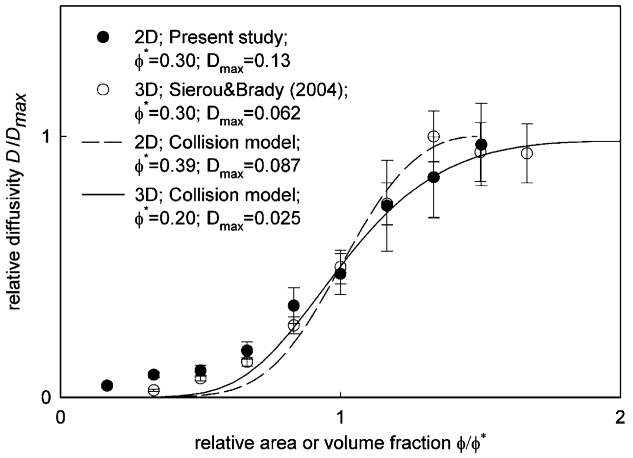

Fig. 10. Comparison of the shear-induced diffusivity as predicted by the collision model and by computer simulation. The shear-induced diffusivity D_{yy} and the area or volume fraction ϕ are normalised following scaling rules derived from the results of the collision model. The values for ϕ^* and $D_{\max}$ are determined separately for each curve from the results presented in Figs. 7 and 9. For the 2D results of the present study, the value for $D_{\max}$ is derived from D_{yy} at ϕ^*.

Based on this understanding, our expectations for 2D systems are that at relatively low area fractions, the shear-induced diffusion component D_{yy} is smaller than for 3D systems. At area fractions above 0.25, the 2D diffusion component can become up to a factor 3.5 higher, due to the difference in area/volume fraction dependence. A normalisation was carried out by dividing the area or volume fraction by ϕ^*, the fraction where the diffusivity has reached half of the maximal value ($0.5D_{\max}$), and by dividing the diffusivity by its maximal value ($D_{\max}$) (Fig. 10). As a result, the normalised 2D and 3D values of the collision model nicely coincide with each other. The same procedure has been carried out on the 2D and 3D simulation results, but here, because the collision model did not capture the $D_{yy} - \phi$ relation well, the normalisation parameters were derived from the simulation results itself. In this way, a good agreement is found between the normalised data of our 2D LB simulations and the 3D Stokesian dynamics simulations of Sierou and Brady (2004). This indicates that the 2D–3D scaling relation as determined from the collision model, is suited for the translation of (future) 2D simulation results to 3D.

5. Conclusions

In this study, we have analysed the flow behaviour of suspensions subjected to Couette flow, making use of the LB method. The focus was on a comparison of the flow behaviour of 2D and 3D suspensions. Since computations on 3D suspensions can computationally be very intensive, it is investigated whether and when it is advantageous to carry out computations on 2D suspensions and translate these results to 3D suspensions with the help of scaling relations.

We have found particle structuring near the walls in both 2D and 3D suspensions. The thickness of the structuring layer was thinner for 3D suspensions, which is in accordance with wall effects in 2D and 3D single particle systems. Wall slip was found in both systems as well, and was more intensive in 3D systems and at higher concentrations. An important consequence of the differences between 2D and 3D is that when one is interested in the bulk particle behaviour, in the 2D system, a larger system size should be chosen than in a 3D system.

For computation of the viscosity and shear-induced diffusion, limitations are found in the maximum volume fraction of particles that gives accurate results; these limitations are found to be related to the grid size of the suspended particles. In 3D systems, for a particle radius of 8 lattice units, the inaccuracy became evident at ϕ larger than 0.30 (viscosity) or larger than 0.15 (shear-induced diffusion), which is at much lower concentrations than in 2D systems. This sensitivity of 3D systems to inaccuracy is probably related to the closer approach distance of two interacting particles in shear flow and may be caused by inaccuracy, introduced by the particle discretisation on the grid.

Because of the very large particle grid sizes, necessary to obtain accurate results for 3D systems, only advanced supercomputers are currently suited for LB computations on 3D systems, while the computations on 2D systems can be carried out well on a single processor or on small computer clusters. Therefore, adequate scaling relations would be helpful to translate 2D simulation results to 3D systems. For the viscosity, such scaling relations are already known, and we were able to reproduce those in our LB simulations. For shear-induced diffusion, we have developed an analytical collision model, which is able to predict qualitatively correct shear-induced diffusivities, and which captures the scaling between 2D and 3D well.

This study shows that the feasibility of 3D LB simulations is restricted to smaller parameter domains than 2D simulations. With the use of relatively simple, linear scaling rules, it proved possible to translate 2D simulation results to 3D real systems, which opens the way to employ the LB method for unexplored aspects of suspension flow in Couette systems, such as particle polydispersity and high Reynolds number flow, with large relevance to practical processing of suspensions.

Acknowledgements

Friesland Foods is greatly acknowledged for supporting this research. Prof. Dr. Mike Cates and Dr. Kevin Stratford from Edinburgh University are greatly thanked for fruitful discussions. The authors would like to acknowledge the support of the Dutch Ministries of Economic Affairs, Education, Culture and Sciences and of Housing, Spatial Planning and the Environment through a grant of the Dutch Program Economy, Ecology and Technology and the support of the European Commission through Grant number HPRI-CT-1999-00026 (the TRACS Programme at EPCC).

Appendix A. Lubrication force in a 2D suspension

We apply lubrication theory to calculate the hydrodynamic force between two cylinders in a 2D suspension. For small gaps (i.e., rim to rim distances) $2h$ the force between two adjacent cylinders can be calculated, solving the flow field in the gap upto first order in $\varepsilon = h/a$. In the calculation two cylinders are considered, approaching each other with a velocity $2U$. A Carthesian coordinate system ($\mathbf{e_x}$, $\mathbf{e_z}$) was used with the origin at the center of the gap. The z-coordinate, taken along the line of centers, was scaled on h and the x-coordinate was scaled on $\sqrt{ah}$; the z-component of the velocity was scaled on U, the x-component on $\sqrt{a/h}U$. The pressure was scaled on $a\eta U/h^2$. Under these conditions the differential equation for the dimensionless stream function ψ becomes

$$\frac{\partial^4\psi}{\partial z^4} + 2\varepsilon\frac{\partial^4\psi}{\partial x^2\partial z^2} + \varepsilon^2\frac{\partial^4\psi}{\partial x^4} = 0. \tag{A.1}$$

The rim of both disks is described by $z = \pm b(x)$ with

$$b(x) = 1 + \tfrac{1}{2}x^2 + \varepsilon\tfrac{1}{8}x^4 + \varepsilon^2\tfrac{1}{16}x^6 + \cdots \tag{A.2}$$

and the boundary conditions on these rims read:

$$v_z = -\frac{\partial\psi}{\partial x} = \pm 1, \tag{A.3}$$

$$v_x = \frac{\partial\psi}{\partial z} = 0. \tag{A.4}$$

For convenience $\psi = 0$ is chosen at $z = 0$, so ψ is odd in z. This equation can be solved assuming

$$\psi = \psi_0 + \varepsilon\psi_1 + \cdots, \tag{A.5}$$

where ψ_0 fulfills the boundary conditions (A.3) and (A.4) and $\partial\psi_1/\partial x = \partial\psi_1/\partial z = 0$ on the rim of the particle. The solution is given by

$$\psi_0 = \frac{1}{2}x\left(3\left(\frac{z}{b}\right) - \left(\frac{z}{b}\right)^3\right), \tag{A.6}$$

$$\psi_1 = \frac{3}{20}g(x)\left(\frac{z}{b}\right)\left(1 - \left(\frac{z}{b}\right)^2\right)^2, \tag{A.7}$$

where $g(x) = 4x(b')^2 - 2bb' - xbb''$ and b', b'' are the first and second derivative of $b = b(x)$, respectively. The pressure along the line $z = 0$ can be calculated by integrating:

$$\left(\frac{\partial p}{\partial x}\right)_{z=0} = -3b^{-3}\left(x + \varepsilon\left(\frac{3}{5}g(x) - \frac{1}{2}f(x)\right)\right), \tag{A.8}$$

where $f(x) = 2x(b')^2 - 2bb' - xbb''$. The zz-component of the total stress tensor (the superfix $^{[D]}$ indicates the dimensional form)

$$T_{zz}^{[D]} = -p^{[D]} + 2\eta \frac{\partial v_z^{[D]}}{\partial z^{[D]}}$$

reads in dimensionless form

$$T_{zz} = -p + 2\varepsilon \frac{\partial v_z}{\partial z} = -p - 2\varepsilon \frac{\partial^2 \Psi}{\partial x \partial z},$$

where also T_{zz} has been scaled on $p_0 = a\eta U/h^2$. The (dimensionless) force per unit length, F, on the particle is calculated by integrating T_{zz} along the line $z = 0$ (with swopping the order of integration of the $\partial p/\partial x$ term):

$$\begin{aligned} F(\varepsilon) &= 2\int_0^\infty (T_{zz})_{z=0}\,\mathrm{d}x \\ &= 2\int_0^\infty x\left(\frac{\partial p}{\partial x}\right)_{z=0}\mathrm{d}x - 4\varepsilon\int_0^\infty \left(\frac{\partial^2 \Psi}{\partial x \partial z}\right)_{z=0}\mathrm{d}x \\ &= \int_0^\infty \frac{3x}{b^3(x)}\left(2x + \varepsilon\left(\frac{6}{5}g(x) - f(x)\right)\right)\mathrm{d}x \\ &\quad - 4\varepsilon\int_0^\infty \frac{3}{2b^2}(b - xb')\,\mathrm{d}x. \end{aligned} \tag{A.9}$$

This expression can be rewritten as

$$F(\varepsilon) = F_0 + \varepsilon(F_1 - F_2),$$

where

$$F_0 = \int_0^\infty \frac{6x^2}{\left(1 + \frac{1}{2}x^2\right)^3}\,\mathrm{d}x = \frac{3}{4}\pi\sqrt{2} = 3.3322,$$

$$F_1 = \int_0^\infty \frac{3x}{\left(1 + \frac{1}{2}x^2\right)^3}\left(\left(\frac{25}{10}x^3 - \frac{3}{5}x - \frac{6x^5}{(8+4x^2)}\right)\right)\mathrm{d}x,$$

$$= \frac{207}{80}\pi\sqrt{2} = 11.496,$$

$$F_2 = \int_0^\infty 6\frac{\left(1 - \frac{1}{2}x^2\right)}{\left(1 + \frac{1}{2}x^2\right)^2}\,\mathrm{d}x = 0.0$$

are numerical constants. In our simulations, we have erroneously used a value of $F_1 = 12.829$, which lead to about 1% overestimation of the lubrication force. The lubrication force per unit length in dimensional form, $F^{[D]} = p_0\sqrt{ah}F$, follows from Eq. (A.9) as

$$\begin{aligned} F^{[D]} &= \left(\frac{h}{a}\right)^{-3/2}\eta U F(h/a) \\ &= \left(\frac{h}{a}\right)^{-3/2}\eta U\left(F_0 + \frac{h}{a}F_1\right) \end{aligned} \tag{A.10}$$

which expression is correct to the first order of ε.

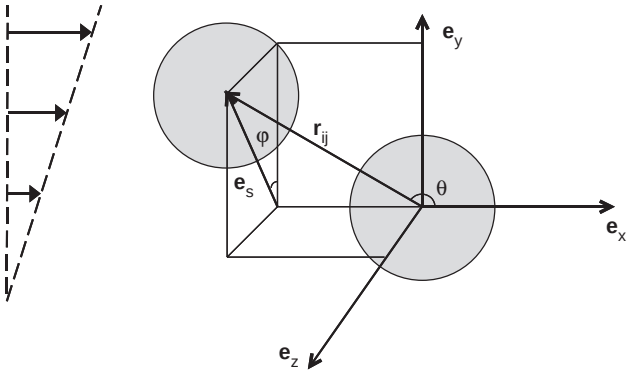

Fig. B.1. Geometry for describing a typical collision.

Appendix B. Analytical model for shear-induced diffusion

B.1. The collision frequency of the particle in 3D

Consider a simple shear field in which the velocity of the fluid (in Carthesian coordinates) is given by

$$\mathbf{v} = \dot{\gamma} y \mathbf{e}_x \tag{B.1}$$

so the x-direction is the velocity direction, the y-direction along the gradient and the z-direction along the vorticity direction. A collision takes place when two particles touch each other: $r_{ij} = p = a_i + a_j$, where a_i is the radius of particle (i).

Using spherical coordinates (r, ϑ, φ) (see Fig. B.1) and the unit vectors:

$$\begin{aligned} \mathbf{e}_r &= -\cos\vartheta\,\mathbf{e}_x + \sin\vartheta\,\mathbf{e}_s, \\ \mathbf{e}_\vartheta &= \sin\vartheta\,\mathbf{e}_x + \cos\vartheta\,\mathbf{e}_s, \\ \mathbf{e}_\varphi &= -\sin\varphi\,\mathbf{e}_y + \cos\varphi\,\mathbf{e}_z, \end{aligned} \tag{B.2}$$

where $\mathbf{e}_s$ is defined by

$$\mathbf{e}_s = \cos\varphi\,\mathbf{e}_y + \sin\varphi\,\mathbf{e}_z \tag{B.3}$$

the relative position between two particles is given by

$$\mathbf{r}_{\mathrm{rel}} = p(-\cos\vartheta\,\mathbf{e}_x + \sin\vartheta\,\mathbf{e}_s) \tag{B.4}$$

and the relative velocity before collision by

$$\mathbf{v}_{\mathrm{rel}} = \dot{\gamma} p \sin\vartheta\,\cos\varphi\,\mathbf{e}_x. \tag{B.5}$$

We consider a monodisperse suspension with volume fraction ϕ of particles with radius a. The particle flux onto the surface of a tagged particle can be estimated as

$$\mathbf{j} = n\mathbf{v}_{\mathrm{rel}} = 2na\dot{\gamma}\sin\vartheta_o\cos\varphi_o\mathbf{e}_x \tag{B.6}$$

where n is the number density of the particles in the suspension. ϑ_o and φ_o define the orientation of the colliding particles. The collision rate in a certain space angle $\mathrm{d}\dot{N}_c/\mathrm{d}\Omega$

is given by

$$\mathrm{d}\dot{N}_c = -n\mathbf{v}_{\mathrm{rel}} \cdot (2a)^2 \,\mathrm{d}\Omega\, \mathbf{e}_r, \tag{B.7}$$

$$\frac{\mathrm{d}\dot{N}_c}{\mathrm{d}\Omega} = 8na^3\dot{\gamma}\cos\varphi_o \sin\vartheta_o \cos\vartheta_o \tag{B.8}$$

and the total collision rate

$$\dot{N}_c = 2\int_{\Omega^{(1)}} \frac{\mathrm{d}\dot{N}_c}{\mathrm{d}\Omega}\,\mathrm{d}\Omega \tag{B.9}$$

$$= \frac{12}{\pi}\,\phi\dot{\gamma}\int_0^{\pi/2} \sin^2\vartheta_o \cos\vartheta_o \,\mathrm{d}\vartheta_o \int_{-\pi/2}^{\pi/2} \cos\varphi_o \,\mathrm{d}\varphi_o \tag{B.10}$$

$$= \frac{8}{\pi}\,\dot{\gamma}\phi, \tag{B.11}$$

where $\Omega^{(1)}$ is the space angle for which $0 < \vartheta < \pi/2$ and $-\pi/2 < \phi < \pi/2$. The probability that a given collision occurs with orientation (ϑ_o, φ_o) or $(\pi - \vartheta_o, \pi + \varphi_o)$ is given by the function $\Phi(\vartheta_o, \varphi_o)$:

$$\Phi(\vartheta_o, \varphi_o) = \frac{(\mathrm{d}\dot{N}_c/\mathrm{d}\Omega)}{\int_{\Omega^{(1)}} (\mathrm{d}\dot{N}_c/\mathrm{d}\Omega)\,\mathrm{d}\Omega} = \frac{3}{2}\cos\varphi_o \cos\vartheta_o \sin\vartheta_o \tag{B.12}$$

and the mean time, τ, between two collisions of particle 1 with another particle follows from Eq. (B.11):

$$\tau = 1/\dot{N}_c = \frac{\pi}{8\dot{\gamma}\phi}. \tag{B.13}$$

B.2. The collision frequency of a particle in 2D

In 2D the collision rate under a certain angle $\mathrm{d}\dot{N}_c/\mathrm{d}\vartheta$ is given by

$$\mathrm{d}\dot{N}_c = -n\mathbf{v}_{\mathrm{rel}} \cdot 2a\,\mathrm{d}\vartheta\,\mathbf{e}_r, \tag{B.14}$$

$$\frac{\mathrm{d}\dot{N}_c}{\mathrm{d}\vartheta} = 4na^2\dot{\gamma}\sin\vartheta_o\cos\vartheta_o \tag{B.15}$$

and the total collision rate:

$$\dot{N}_c = 2\int_0^{\pi/2} \frac{\mathrm{d}\dot{N}_c}{\mathrm{d}\vartheta}\,\mathrm{d}\vartheta = \frac{8}{\pi}\,\phi\dot{\gamma}\int_0^{\pi/2} \sin\vartheta_o\cos\vartheta_o\,\mathrm{d}\vartheta_o \tag{B.16}$$

$$= \frac{4}{\pi}\,\dot{\gamma}\phi \tag{B.17}$$

hence, in 2D

$$\Phi(\vartheta_o) = 2\cos\vartheta_o \sin\vartheta_o \tag{B.18}$$

and

$$\tau = 1/\dot{N}_c = \frac{\pi}{4\dot{\gamma}\phi}. \tag{B.19}$$

B.3. The displacement of the particle in a collision

To describe the displacement of a particle (i) during a collision with particle (j) we describe the collision with respect to the center of resistance of the two colliding particles. The initial position of particle (i) is given by ϑ_o, φ_o (in 2D: $\varphi_o = 0$): $\mathbf{r}_{cm} = a(-\cos\vartheta_o\mathbf{e}_x + \sin\vartheta_o\mathbf{e}_s(\varphi))$. To obtain a simple collision rule we assume affine motion of the particles as not prohibited by excluded volume effects. When the particles become into contact they roll over each other in the *xs*-plane. Under this assumption the velocity during the collision, $\vartheta_o \leqslant \vartheta \leqslant \vartheta_1$, is

$$\mathbf{v} = \mathbf{v}_\infty \cdot (\mathbf{I} - \mathbf{e}_r\mathbf{e}_r) \tag{B.20}$$

$$= a\dot{\gamma}\cos\varphi_o \sin^2\vartheta(\sin\vartheta\,\mathbf{e}_x + \cos\vartheta\,\mathbf{e}_s) \tag{B.21}$$

while the undisturbed velocity would be given by

$$\mathbf{v}_\infty = a\dot{\gamma}\cos\varphi_o\sin\vartheta\,\mathbf{e}_x. \tag{B.22}$$

The angular speed $\dot{\vartheta}$ is given by: $\dot{\vartheta} = \dot{\gamma}\cos\varphi_o\sin^2\vartheta$ so the time a collision takes, is given by

$$\Delta t = \frac{1}{\dot{\gamma}\cos\varphi_o}\int_{\vartheta_o}^{\vartheta_1} \frac{\mathrm{d}\vartheta}{\sin^2\vartheta} = \frac{(\cot\vartheta_0 - \cot\vartheta_1)}{\dot{\gamma}\cos\varphi_o}, \tag{B.23}$$

where ϑ_1 is the value of ϑ at which the collision stops, $\vartheta_1 = \pi - \vartheta_0$, or is taken over by the next collision:

$$\cot\vartheta_1 = \begin{cases} -\cot\vartheta_0 & \left(\dfrac{2\cot\vartheta_0}{\dot{\gamma}\cos\varphi_o} \leqslant \tau\right), \\ \cot\vartheta_0 - \dot{\gamma}\tau\cos\varphi_o & \left(\dfrac{2\cot\vartheta_0}{\dot{\gamma}\cos\varphi_o} > \tau\right). \end{cases} \tag{B.24}$$

Assuming a collision stops at a certain angle ϑ_1 irrespective of the initial values of ϑ_0 and φ_o, the average collision time in 3D is calculated as

$$\langle\Delta t\rangle = 3\int_0^{\pi/2}\int_0^{\pi/2} \frac{(\cot\vartheta_0 - \cot\vartheta_1)}{\dot{\gamma}\cos\varphi_o} \times \cos\varphi_o\cos\vartheta_o\sin^2\vartheta_o\,\mathrm{d}\vartheta_o\,\mathrm{d}\varphi_o \tag{B.25}$$

$$= \frac{\pi}{2\dot{\gamma}}(1 - \cot\vartheta_1) \tag{B.26}$$

and in 2D as

$$\langle\Delta t\rangle = 2\int_0^{\pi/2} \frac{(\cot\vartheta_0 - \cot\vartheta_1)}{\dot{\gamma}}\cos\vartheta_o\sin\vartheta_o\,\mathrm{d}\vartheta_o \tag{B.27}$$

$$= \frac{1}{\dot{\gamma}}\left(\frac{\pi}{2} - \cot\vartheta_1\right). \tag{B.28}$$

The displacement $\Delta\mathbf{r}$ can be obtained from integration, from time 0 to τ, of the velocity (Eq. (B.20)):

$$\Delta\mathbf{r} = \int_0^{\Delta t}\mathbf{v}(\vartheta, \varphi_0)\,\mathrm{d}t + \int_{\Delta t}^{\tau}\mathbf{v}_\infty(\vartheta_1, \varphi_0)\,\mathrm{d}t + \mathbf{v}_{cm}\tau$$

$$= a\int_{\vartheta_0}^{\vartheta_1}(\sin\vartheta\,\mathbf{e}_x + \cos\vartheta\,\mathbf{e}_s(\varphi_0))\,\mathrm{d}\vartheta + \int_{\Delta t}^{\tau} a\dot{\gamma}\cos\varphi_o\sin\vartheta_1\mathbf{e}_x\,\mathrm{d}t + \mathbf{v}_{cm}\tau,$$

where $\mathbf{v}_{cm}$ is given by:

$$\mathbf{v}_{cm} = \dot{\gamma}(y_0 - a\sin\vartheta_0\cos\varphi_o)\,\mathbf{e}_x.$$

The stochastic part of the displacement $\mathbf{s}$ can be obtained by subtraction of the convective contribution to $\Delta\mathbf{r}$:

$$\Delta\mathbf{r}_c = \tfrac{1}{2}\,\dot{\gamma}\tau(y_0 + y_1)\mathbf{e}_x$$

which results in:

$$\mathbf{s} = \int_0^{\Delta t}\mathbf{v}(\vartheta,\varphi_0)\,\mathrm{d}t + \int_{\Delta t}^{\tau}\mathbf{v}_\infty(\vartheta_1,\varphi_0)\,\mathrm{d}t + \dot{\gamma}\tau(y_0 - a\sin\vartheta_0\cos\varphi_o)\mathbf{e}_x - \tfrac{1}{2}\,\dot{\gamma}\tau(y_0 + y_1)\mathbf{e}_x.$$

In these expressions is Δt given by: $\Delta t = \min\{\tau, (2\cot\vartheta_0)/(\dot{\gamma}\cos\varphi_o)\}$. Hence, for $((2\cot\vartheta_0)/\dot{\gamma}\cos\varphi_o \leqslant \tau)$ one obtains:

$$\mathbf{s} = 0$$

and for $((2\cot\vartheta_0/\dot{\gamma}\cos\varphi_o) > \tau)$:

$$\mathbf{s}/a = [\sin\vartheta_1 - \sin\vartheta_0]\mathbf{e}_s + [\cos\vartheta_0 - \cos\vartheta_1 - \tfrac{1}{2}(\sin\vartheta_0 + \sin\vartheta_1)(\cot\vartheta_0 - \cot\vartheta_1)]\mathbf{e}_x, \qquad \text{(B.29)}$$

where we have used:

$$\dot{\gamma}\tau\cos\varphi_o = \cot\vartheta_0 - \cot\vartheta_1$$

(in 2D the obtained expressions for the displacements are valid if one substitutes $\varphi_o = 0$).

B.4. The self-diffusion tensor

The self-diffusion tensor $\mathbf{D}$ for a particle can be calculated from:

$$\mathbf{D} = \frac{\langle\mathbf{ss}\rangle}{2\tau}. \qquad \text{(B.30)}$$

The averaging has to be done with the weight function Φ (Eq. (B.12)) in the following way:

$$\langle\mathbf{ss}\rangle = \int_{-\pi/2}^{\pi/2}\int_0^{\pi/2}(\mathbf{ss})\Phi(\vartheta_o,\varphi_o)\sin\vartheta_o\,\mathrm{d}\vartheta_o\,\mathrm{d}\varphi_o \qquad \text{(B.31)}$$

$$= 3\int_0^{\pi/2}\int_0^{\pi/2}(\mathbf{ss})\sin^2\vartheta_o\cos\vartheta_o\,\mathrm{d}\vartheta_o\cos\varphi_o\,\mathrm{d}\varphi_o. \qquad \text{(B.32)}$$

The diad $(\mathbf{ss})$ is for $\Delta t = (2\cot\vartheta_0)/(\dot{\gamma}\cos\varphi_o) < \tau$ given by

$$\langle\mathbf{ss}\rangle = a^2\langle\tilde{\mathbf{s}}\,\tilde{\mathbf{s}}\rangle$$

$$\langle\tilde{\mathbf{s}}\,\tilde{\mathbf{s}}\rangle = 3\int_0^{\pi/2}\int_0^{\vartheta_m(\varphi_o)}(\tilde{\mathbf{s}}\,\tilde{\mathbf{s}})\sin^2\vartheta_o\cos\vartheta_o\,\mathrm{d}\vartheta_o\cos\varphi_o\,\mathrm{d}\varphi_o,$$

where $\vartheta_m(\varphi_o) = \arctan(16\phi/(\pi\cos\varphi_o))$. The dyad $(\tilde{\mathbf{s}}\,\tilde{\mathbf{s}})$ is given by

$$\tilde{\mathbf{s}} = [\sin\vartheta_1 - \sin\vartheta_0]\mathbf{e}_s + \cos\vartheta_0 - \cos\vartheta_1 - \tfrac{1}{2}(\sin\vartheta_0 + \sin\vartheta_1)(\cot\vartheta_0 - \cot\vartheta_1)]\mathbf{e}_x \qquad \text{(B.33)}$$

with

$$\cot\vartheta_1 = \cot\vartheta_0 - ((\pi\cos\varphi_o)/8\phi).$$

Finally one obtains an expression for the diffusion tensor:

$$\mathbf{D} = \dot{\gamma}a^2\,\frac{4\phi}{\pi}\,\langle\tilde{\mathbf{s}}\,\tilde{\mathbf{s}}\rangle. \qquad \text{(B.34)}$$

Using Eqs. (B.33) and (B.34) all the components of the self-diffusion tensor can be calculated. In the 2D calculations no φ dependence exists and the weight function Φ is given by Eq. (B.18), while in the expressions for the displacements one has to replace φ_o by 0.

References

Ball, R.C., Melrose, J.R., 1995. Lubrication breakdown in hydrodynamic simulations of concentrated colloids. Advances in Colloid and Interface Science 59, 19–30.

Batchelor, G.K., Green, J.T., 1972. The hydrodynamic interaction of two small freely-moving spheres in a linear flow field. Journal of Fluid Mechanics 56 (2), 375–400.

Behrend, O., 1995. Solid-fluid boundaries in particle suspension simulations via the lattice Boltzmann method. Physical Review E 52 (1), 1164–1175.

Breedveld, L.V.A., 2000. Shear-induced self-diffusion in concentrated suspensions. Ph.D. thesis, University of Twente, The Netherlands.

Breedveld, V., van den Ende, D., Tripathi, A., Acrivos, A.A., 1998. The measurement of the shear-induced particle and fluid tracer diffusivities in concentrated suspensions by a novel method. Journal of Fluid Mechanics 375, 297–318.

Breedveld, V., van der Ende, D., Bosscher, M., Jongschaap, R.J.J., Mellema, J., 2001. Measuring shear-induced self-diffusion in a counterrotating geometry. Physical Review E 63 (021403), 1–10.

Chapman, S., Cowling, T.G., 1960. The Mathematical Theory of Non-uniform Gases. Cambridge University Press, Cambridge.

Da Cunha, F.R., Hinch, E.J., 1996. Shear-induced dispersion in a dilute suspension of rough spheres. Journal of Fluid Mechanics 309, 211–223.

Farr, R.S., Melrose, J.R., Ball, R.C., 1997. Kinetic theory of jamming in hard-sphere startup flows. Physical Review E 55 (6), 7203–7211.

Frankel, N.A., Acrivos, A., 1967. On the viscosity of a concentrated suspension of solid spheres. Chemical Engineering Science 22, 847–853.

Frisch, U., Hasslacher, B., Pomeau, Y., 1986. Lattice-gas automata for the Navier–Stokes equation. Physical Review Letters 56 (14), 1505–1508.

Heemels, M.W., Hagen, M.H.J., Lowe, C.P., 2000. Simulating solid colloidal particles using the Lattice–Boltzmann method. Journal of Computational Physics 164, 48–61.

Komnik, A., Harting, J., 2004. Transport phenomena and structuring in shear flow of suspensions near solid walls. Condense Matter 0408029, 1–13.

Krieger, I.M., 1972. Rheology of monodisperse lattices. Advances in Colloid and Interface Science 3, 111–136.

Krieger, I.M., Dougherty, T.J., 1959. A mechanism for non-Newtonian flow in suspensions of rigid spheres. Transactions of the Society Rheology 3, 137–152.

Kromkamp, J., van den Ende, D.T.M., Kandhai, D., van der Sman, R.G.M., Boom, R.M., 2005. Shear-induced self-diffusion and microstructure in non-Brownian suspensions at non-zero Reynolds numbers. Journal of Fluid Mechanics 529, 253–278.

Ladd, A.J.C., 1994a. Numerical simulations of particulate suspensions via a discretized Boltzmann equation. Part 1. Theoretical foundation. Journal of Fluid Mechanics 271, 285–309.

Ladd, A.J.C., 1994b. Numerical simulations of particulate suspensions via a discretized Boltzmann equation. Part 2. Numerical results. Journal of Fluid Mechanics 271, 311–339.

Ladd, A.J.C., Verberg, R., 2001. Lattice–Boltzmann simulations of particle-fluid suspensions. Journal of Statistical Physics 104 (5/6), 1191–1251.

Leighton, D., Acrivos, A., 1987. The shear-induced migration of particles in concentrated suspensions. Journal of Fluid Mechanics 181, 415–439.

Nguyen, N.-Q., Ladd, A.J.C., 2002. Lubrication corrections for Lattice–Boltzmann simulations of particle suspensions. Physical Review E 66 (046708), 1–12.

Nirschl, H., Dwyer, H.A., Denk, V., 1995. Three-dimensional calculations of the simple shear flow around a single particle between two moving walls. Journal of Fluid Mechanics 283, 273–285.

Phillips, R.J., Armstrong, R.C., Brown, R.A., Graham, A.L., Abbott, J.R., 1992. A constitutive equation for concentrated suspensions that accounts for shear-induced particle migration. Physics of Fluids A 4, 30–40.

Qian, Y.H., d'Humières, D., Lallemand, P., 1992. Lattice BGK models for the Navier–Stokes equation. Europhysics Letters 17, 479–484.

Shakib-Manesh, A., Raiskinmäki, P., Koponen, A., Kataja, M., Timonen, J., 2002. Shear stress in a Couette flow of liquid-particle suspensions. Journal of Statistical Physics 107 (1/2), 67–84.

Sierou, A., Brady, J.F., 2004. Shear-induced self-diffusion in non-colloidal suspensions. Journal of Fluid Mechanics 506, 285–314.

Succi, S., 2001. The Lattice Boltzmann Equation for Fluid Dynamics and Beyond. Oxford University Press, New York.

Taylor, G.I., 1932. The viscosity of a fluid containing small drops of another fluid. Proceedings of the Royal Society London A 138 (834), 41–48.